Non-ideal Effects in Compressible Swirling Flows

Francesco Tosto, Andrea Giuffre', Piero Colonna, and Matteo Pini(✉)

Propulsion and Power, Delft University of Technology, Delft, The Netherlands
m.pini@tudelft.nl

Abstract. In this work we examine the behavior of non-ideal compressible swirling flows. Based on a first-principle analysis, we derive a generalized expression of the corrected flow per unit area as function of the isentropic exponent, characteristic Mach numbers, and swirl parameter. The calculated trends of the corrected flow with respect to these parameters, validated against results from high-fidelity computations, are used to infer physical insights on the behavior of swirling flows in turbomachinery cascades. The results suggest that fluid flows characterized by low values of the isentropic exponent show swirling behaviors that are substantially different than those exhibited by perfect gases. Ultimately, this can make the design of efficient turbomachines operating close to the critical point particularly challenging.

Keywords: Isentropic exponent · Swirling flow · Corrected flow function

1 Introduction

Swirling flows, namely flows characterized by a non-negligible circumferential velocity component, are ubiquitous in internal flow devices. Swirling in turbomachines is typically induced by the circumferential motion the flow is subject to when passing through a blade row or a radial vaneless duct, e.g. a radial diffuser. The combination of swirl and compressibility in turbomachinery leads to flow features beyond those encountered in the examination of either phenomenon separately and that can have large impact on their performance. The key parameter governing the behavior of a turbomachinery stage is the well-known corrected flow per unit area, which is a direct measure of its flow capacity [3]. This quantity is used to determine, among others, the response of a swirling flow to changes in passage area and is thus highly suited to characterize the actual behavior of a turbomachine stage, as for instance its choking condition. As outlined in recent works [2,7] compressibility effects in turbomachinery blade rows operating in the non-ideal compressible flow regime can be greatly enhanced or mitigated depending on whether the so-called generalized isentropic exponent [5] is higher or lower than the heat capacity ratio of the fluid in the limit of dilute gas. The occurrence of non-ideal gas effects in swirling flows is then expected to have large impact on the choking condition of a turbomachinery stage, thus on the value of the corrected flow per unit area. This paper presents a fundamental investigation aimed at examining,

M. Pini et al. (Eds.): NICFD 2020, ERCOFTAC Series 28, pp. 36–43, 2021.
https://doi.org/10.1007/978-3-030-69306-0_5

from a qualitative standpoint, characteristic features of isentropic non-ideal compressible swirling flows typically encountered in turbomachines with the ultimate goal of revealing potential opportunities for their optimal design.

2 Background

Figure 1 shows the schematic of a typical swirling flow configuration and the nomenclature used throughout the paper. The canonical expression of the corrected flow per unit area for ideal gas flows [3] can be rearranged to highlight the role of the swirl velocity component. The canonical equation reads

$$\dot{m}_{\text{corr}} = \frac{\dot{m}\sqrt{RT_{\text{t}}}}{p_{\text{t}}A\sqrt{\gamma}} = \sqrt{\frac{T}{T_{\text{t}}}}\frac{\rho}{\rho_{\text{t}}}\frac{u_m}{\sqrt{\gamma RT_{\text{t}}}} = M_{\text{m}}f(M), \tag{1}$$

where M_{m} is the meridional Mach number. By introducing the generalized isentropic exponent, defined as

$$\gamma_{pv} = -\frac{v}{p}\left(\frac{\partial p}{\partial v}\right)_s = -\frac{v}{P}\frac{c_p}{c_v}\left(\frac{\partial P}{\partial v}\right)_T, \tag{2}$$

and related to the fundamental derivative of gas dynamics Γ [8] through the relation [4]

$$\Gamma = \frac{1}{2}\left[\gamma_{pv} + 1 - \frac{v}{\gamma_{pv}}\left(\frac{\partial \gamma_{pv}}{\partial v}\right)_s\right], \tag{3}$$

one can rewrite (1) as function of γ_{pv} or Γ. When the fluid state is sufficiently far from the critical point, the partial derivative in Eq. 3 can be neglected and a linear trend of γ_{pv} with Γ is established. Such approximation has been exploited, for example, in the studies documented in [2,9].

By using the same approximation, Eq. (1) can therefore be casted in a form that is suited to point out the effect of flow non-ideality. By resorting to the generalized isentropic exponent γ_{pv} [2], this yields

$$\dot{m}_{\text{corr}} = \frac{\dot{m}\sqrt{Z_{\text{t}}RT_{\text{t}}}}{p_{\text{t}}A\sqrt{\gamma_{pv}}} = \frac{M_m}{\left(1+\frac{\gamma_{pv}-1}{2}M^2\right)^{\frac{\gamma_{pv}+1}{2(\gamma_{pv}-1)}}}, \tag{4}$$

where $Z_{\text{t}} = p_{\text{t}}/(\rho_{\text{t}}RT_{\text{t}})$ is the flow compressibility factor defined at total conditions. Eventually, after further algebraic manipulation

$$\dot{m}_{\text{corr}} \simeq \frac{\dot{m}}{\rho_{\text{t}}c_{\text{t}}A} = \left(1+\frac{\gamma_{pv}-1}{2}M^2\right)\sqrt{\frac{M^2}{1+\frac{\gamma_{pv}-1}{2}M^2} - \left(\frac{u_\theta}{\sqrt{\gamma_{pv,\text{t}}Z_{\text{t}}RT_{\text{t}}}}\right)^2}, \tag{5}$$

where the second term under the square root is referred to as swirling parameter and denotes the amount of swirl of a given flow. Equation 5 clearly shows the relation

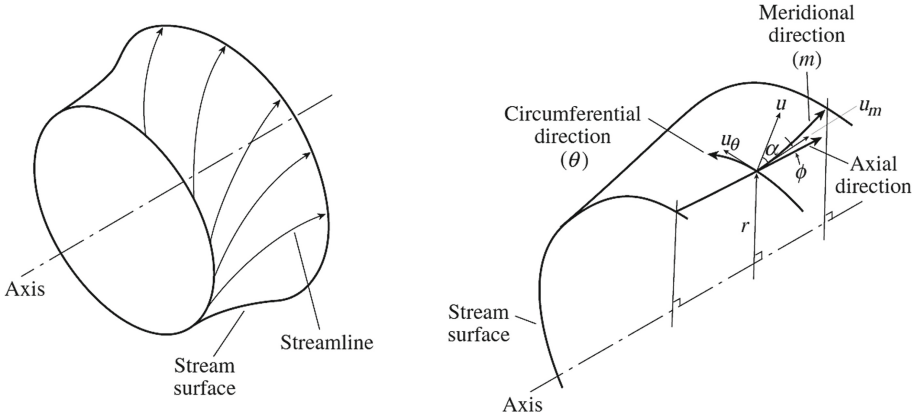

Fig. 1. Axisymmetric swirling flow in a duct with variable cross section and coordinate system [3].

between the corrected flow per unit area and the swirling parameter. Using the isentropic relation $p_t/p = f(M, \gamma_{pv})$, Eq. 4 can also be rewritten in terms of pressure ratio and flow (swirl) angle, namely

$$\dot{m}_{\text{corr}} = \left(\frac{p_t}{p}\right)^{\frac{\gamma_{pv}+1}{2\gamma_{pv}}} \sqrt{\frac{2}{\gamma_{pv}-1}\left[\left(\frac{p}{p_t}\right)^{\frac{1-\gamma_{pv}}{\gamma_{pv}}} - 1\right]} \cos\alpha. \tag{6}$$

Note that the accuracy of the results obtained by applying the above equations depends on the actual variation of γ_{pv} along an expansion process and is therefore related to the extent of flow non-ideality, namely on the relative difference between γ and γ_{pv}, and to the flow Mach number.

3 Technical Approach

Equations (5) and (6) constitute the analytical models used to investigate the impact of non-ideal flow effects on the behavior of swirling flows. The study is performed by considering expansion processes occurring in an exemplary turbomachine operating with a paradigmatic fluid that can exhibit substantial variability of degree of non-ideality, herein evaluated as the deviation of γ_{pv} from γ of the fluid in the dilute gas state. The contours of γ_{pv} for siloxane MM and CO_2 are shown in Fig. 2 to illustrate the range of variation of the isentropic exponent for hypothetical expansion processes occurring in the non-ideal compressible flow regime. For instance, pre-expansion processes at the impeller inlet of supercritical CO_2 compressors usually occur in thermodynamic regions where $\gamma_{pv} > \gamma$, while flow expansions in an ORC turbine operating with MM can entail values of γ_{pv} lower or higher than γ. Table 1 lists the main fluid properties of the two fluids under investigation along with the lower and upper values of γ_{pv} occurring in the thermodynamic region bounded by $p < 2.5p_{cr}$ and $s > s_{cr}$. Note that the higher the

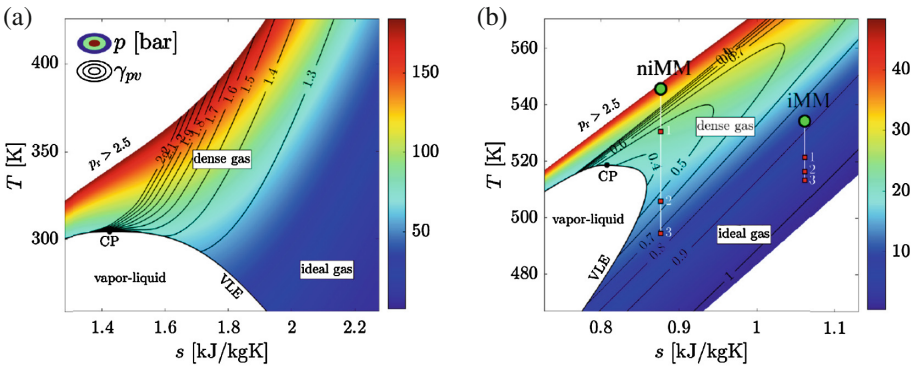

Fig. 2. Thermodynamic temperature-entropy diagrams of CO_2 (a) and siloxane MM (b). Pressure and γ_{pv} contours are reported. CP and VLE denote critical point and saturation vapor-liquid curve. Isentropic processes iMM and niMM discussed in Sect. 4.2 are reported in figure (b).

Table 1. Characteristic fluid properties of air, carbon dioxide and siloxane MM. γ_∞ is the specific heat ratio calculated in the dilute gas state. The lower and upper bound of γ_{pv} are those occurring in the thermodynamic region defined by $s > 1.01 s_{cr}$ and by the thermal stability limits of each molecule.

	M_{mol} [kg/kmol]	T_{cr} [K]	p_{cr} [bar]	γ_∞	$\gamma_{pv,min}$	$\gamma_{pv,max}$
Air	28.96	132.82	38.50	1.40	1.44	2.85
CO2	44.01	304.13	73.77	1.29	0.86	4.33
MM	162.3	518.70	19.31	1.03	0.39	4.75

molecular complexity of the fluid, the lower the γ_{pv} value that the fluid exhibits in the considered thermodynamic region. Furthermore, fluids made by complex molecules can feature a non monotonic trend of γ_{pv} along an isentropic process, as shown in Fig. 2b.

The trends of the corrected flow per unit area are computed as a function of M_m or pressure ratio p/p_t and for different values of total Mach number M, swirl angle α, and normalized swirl velocity component $\hat{u}_\theta = u_\theta / \sqrt{\gamma_{pv,t} Z_t R T_t}$.

4 Results

4.1 Physical Insights

Figure 3 shows the trend of corrected flow per unit area as a function of the meridional Mach number for three values of generalized isentropic exponent γ_{pv}. In the charts, lines of constant total Mach number, flow angle, and swirl parameter are also displayed. Several physical insights relevant to turbomachinery applications can be derived from inspection of these charts.

First, it can be seen that the vertical line corresponding to $M_m = 1$ passes through the maxima of the curves at constant $\hat{u}_\theta$. This means that choking in swirling flows is actually reached when the magnitude of the meridional velocity component equals that

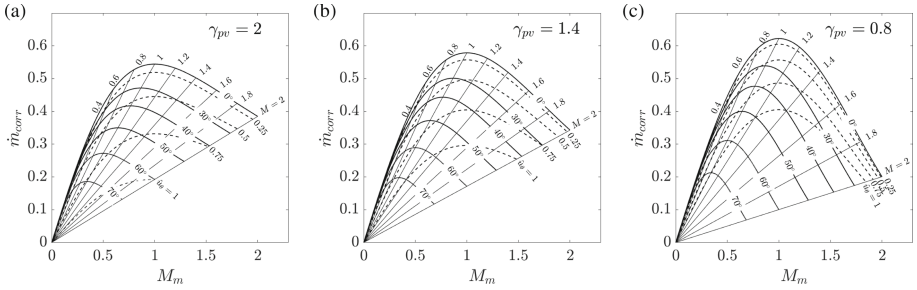

Fig. 3. Corrected mass flow per unit area vs meridional Mach number for different values of total Mach number M, swirl angle α, swirl velocity parameter $\hat{u}_\theta$. Graphs are reported for the cases (a) $\gamma_{pv} = 2$, (b) $\gamma_{pv} = 1.4$ and (c) $\gamma_{pv} = 0.8$.

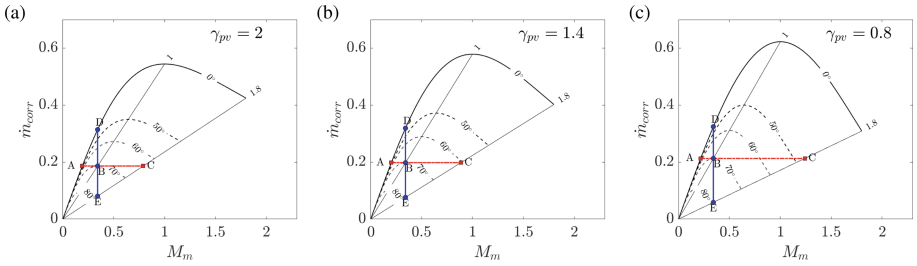

Fig. 4. Characteristic flow state trajectories on the $\dot{m}_{\mathrm{corr}} - M_{\mathrm{m}}$ diagrams. Line A→C illustrates a process at constant $\dot{m}_{\mathrm{corr}}$; line D→E illustrates a process at constant M_{m}. Graphs are reported for the cases (a) $\gamma_{pv} = 2$, (b) $\gamma_{pv} = 1.4$ and (c) $\gamma_{pv} = 0.8$.

of the speed of sound and the flow is already in the supersonic regime, i.e. $M > 1$. The value of total Mach number at which choking occurs strongly depends on the γ_{pv} value. For instance, by assuming $\hat{u}_\theta = 0.75$, choking is achieved at $M \approx 1.2$ for $\gamma_{pv} = 0.8$ and at higher Mach numbers for larger values of γ_{pv}. This finding has important consequences for turbomachinery design. Given that the line at $M_m = 1$ represents the physical limit of operation of a turbomachine vane providing swirl to the flow ($M_m > 1$ would entail the impossibility of the flow to adapt to outlet conditions), it is common practice to design swirling devices in the transonic/supersonic regime with sufficient margin from that limit to avoid controllability issues. If the vane operates in a thermodynamic region whereby $\gamma_{pv} < \gamma$ the condition $M_m = 1$ would be reached sooner, meaning that the component cannot be designed for high total Mach numbers. Conversely, vanes designed to operate in regions whereby, on average, $\gamma_{pv} > \gamma$ can handle highly supersonic flow. However, a quantitative estimate of suitable ranges of Mach number for safe operation could only be estimated once the amount of swirl is known.

The last considerations have important implications in terms of flow behavior within actual turbine cascades. The insights can be better appreciated by examination of Fig. 4, that shows only a subset of the curves previously displayed. The lines A-B-C and D-E identify two different gas-dynamic processes. Notably, the horizontal line A-B-C at

Table 2. Boundary conditions used in the CFD simulations.

	$p_{t,in}$ [bar]	$T_{t,in}$ [K]	$p_{out,1}$ [bar]	$p_{out,2}$ [bar]	$p_{out,3}$ [bar]
iMM	9.66	534.26	4.13	3.44	2.80
niMM	40.00	545.67	22.48	14.45	10.23

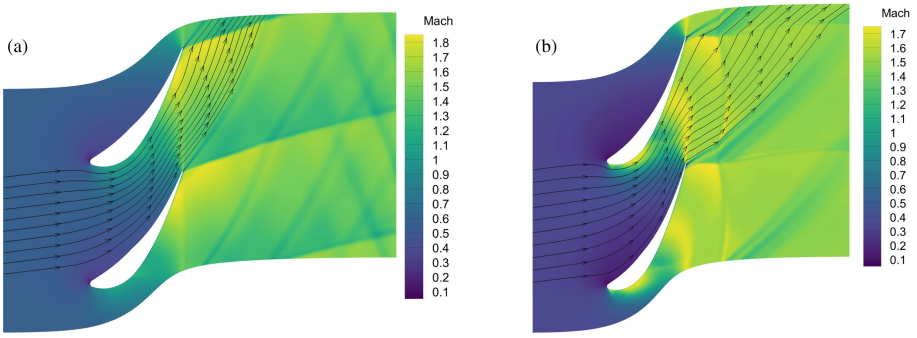

Fig. 5. Mach number contours and streamlines computed by 3D RANS at midspan for (a) iMM, (b) niMM close to chocking (case 3).

constant corrected flow is approximately representative of the initial (point B) and final states of a post-expansion (point C) or post-compression (point A) process occurring downstream of a choked turbine row. Following the line B-C, it can be observed that the flow deflects towards the meridional direction while expanding from choking conditions to $M = 1.8$. The magnitude of the deflection amounts to more than 20° when $\gamma_{pv} = 0.8$ and less than 10° when $\gamma_{pv} = 2.0$. In other words, the flow post-expanding downstream of a turbine row operating in the proximity of the critical point, where $\gamma_{pv} < \gamma$, is subject to deviations that are substantially higher than those that would occur if the same flow behaved as an ideal gas. Because of that, the assumption of small or negligible flow deviation, underlying most of the meanline design methods, is essentially incorrect in non-ideal flow conditions and a careful evaluation of this quantity becomes necessary during early stage of turbomachinery design.

The vertical line D-E exemplifies a flow expansion with the total Mach number increasing from nearly 0.5 to 1.8 at constant $M_m = 0.3$, a behavior qualitatively representative of the flow process in a supersonic axial turbine vane designed at constant flow coefficient and with negligible post-expansion. To achieve this acceleration, the swirl angle rises from 0° to roughly 80° in all cases and the corrected flow reduces because of the corresponding increase of passage area. The reduction of corrected flow and the associated increase of annulus area is more significant as γ_{pv} decreases, as a direct consequence of the increase in volumetric flow ratio ρ_t/ρ. This finding corroborates the previous results in that the design of an efficient turbine row expanding a flow in near-critical thermodynamic conditions is arguably much more challenging to accomplish.

4.2 Verification

Results obtained by means of high-fidelity CFD [1] are utilized to assess the accuracy of the previous trends. 3D RANS computations of the flow past converging turbine vanes designed to operate with siloxane MM in ideal (case iMM) and non-ideal (case niMM) compressible flow regime are performed. The boundary conditions, specified in terms of inlet total pressure, inlet total temperature and outlet average static pressure are reported in Table 2. Turbulence boundary conditions, set in terms of inlet turbulence intensity, eddy viscosity ratio and turbulent Prandtl number, are fixed to reference values for all the simulations: $k = 5\%, \mu/\mu_t = 10, Pr_t = 1$. Total variation diminishing (TVD) schemes are adopted to discretize the advective and turbulent fluxes, while the viscous fluxes are discretized with a central difference scheme. $k-\omega$ SST turbulence model is employed together with adequate cell clustering near walls to guarantee $y^+ < 1$. The thermo-physical fluid properties are evaluated through a look-up table method coupled to the reference thermodynamic library [6]. A grid size of $5 \cdot 10^6$ cells and a look-up table composed by $2.5 \cdot 10^6$ and $4 \cdot 10^6$ elements for case iMM and niMM, respectively, are selected as trade-off between accuracy and computational cost.

The corrected mass flow per unit area is evaluated at midspan radius in three different sections, namely at the inlet, throat and outlet boundaries. The expansion ratio across the blade rows is progressively increased from the design point (case 1) to investigate post-expansion effects (cases 2–3). The average values of γ_{pv} and local flow deflection α computed by CFD at the outlet section are used to evaluate $\dot{m}_{\text{corr}}$ by means of Eq. (6). Figure 6 shows the comparison of the results obtained with the two models, together with the variation of the generalized isentropic exponent along the corresponding isentropic processes depicted in Fig. 2b. Several considerations can be drawn by examination of these charts.

First, provided that there is sufficient margin from the actual chocking limit of the cascade, i.e. up to point 2 for the case niMM, where $M_m \approx 0.9$, predictions made by the analytical models are qualitatively in line with the CFD results. Moreover, CFD trends are in agreement with the analytical results in that a lower variation of $\dot{m}_{\text{corr}}$ from inlet to outlet can be expected when increasing γ_{pv}.

The CFD simulations confirm the validity of the analysis regarding the post-expansion process reported in the previous paragraph. In this regard, the use of converging-diverging blade channels in turbine stages where the target expansion entails an average value of $\gamma_{pv} < \gamma$ can be advantageous to better control the flow deviation rather than to improve the fluid-dynamic efficiency.

Lastly, the ideal expansion process represented in Fig. 4 by the D-B-C line can be compared to the actual expansion in a converging turbine vane designed at constant flow coefficient and operating at off-design, i.e. the points inlet-throat-outlet (2–3) in Fig. 6. One can notice that in the actual expansion process the sonic state is systematically shifted rightwards, since chocking occurs at a lower flow angle than that of point B. In view of this observation, point B can be deemed to reproduce more closely the outlet state at design conditions, i.e. when the post-expansion is negligible and the total Mach number is close to one.

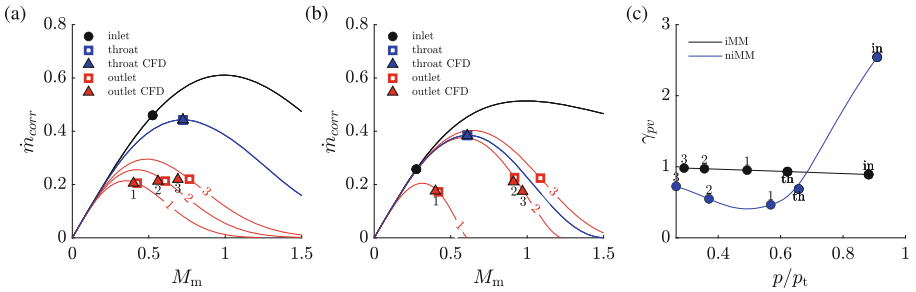

Fig. 6. Validation of test cases (a) iMM and (b) niMM with CFD. $\dot{m}_{\mathrm{corr}}(M_{\mathrm{m}})$ curves in red are computed with values of local flow deflection α and γ_{pv} at the stator outlet obtained from CFD. The black $\dot{m}_{\mathrm{corr}}(M_{\mathrm{m}})$ curve refers to the stator inlet conditions. (c) Variation of γ_{pv} with pressure drop along the isentropic processes iMM and niMM.

5 Conclusions

Non-ideal compressible swirling flows can show behaviors that are substantially different than those exhibited by perfect gases. The results of the work pointed out that, for fluids made by complex molecules, post-expansion effects in turbomachine vanes are greatly enhanced and choking can occur sooner if the expansion process occurs in the proximity of the critical point, where γ_{pv} assume values lower or significantly lower than γ_∞. Further analyses are needed to gain additional physical insights and to determine the relative implications for the optimal design of turbomachinery operating with non-ideal compressible flows.

References

1. ANSYS: Ansys workbench, release 19.3, ANSYS, canonsburg, pa (2019)
2. Baumgärtner, D., Otter, J.J., Wheeler, A.P.S.: The effect of isentropic exponent on transonic turbine performance. J. Turbomach. **142**(8), 081007/1–081007/10 (2020)
3. Greitzer, E.M., Tan, C.S., Graf, M.B.: Internal Flow: Concepts and Applications. Cambridge University Press, Cambridge (2004)
4. Henderson, L.R.F.: General laws for propagation of shock waves through matter. In: Handbook of Shock Waves, pp. 143–183. Elsevier (2001)
5. Kouremenos, D.A., Antonopoulos, K.A.: Isentropic exponents of real gases and application for the air at temperatures from 150k to 450k. Acta Mech. **65**(1), 81–99 (1987)
6. Lemmon, E.W., Bell, I.H., Huber, M.L., McLinden, M.O.: NIST standard reference database 23: Reference fluid thermodynamic and transport properties-REFPROP, version 10.0, National Institute of Standards and Technology (2018)
7. Romei, A., Vimercati, D., Persico, G., Guardone, A.: Non-ideal compressible flows in supersonic turbine cascades. J. Fluid Mech. **882**, A12 (2020)
8. Thompson, P.A.: A fundamental derivative in gasdynamics. Phys. Fluids **14**(9), 1843 (1971)
9. Wheeler, A.P.S., Ong, J.: The role of dense gas dynamics on organic rankine cycle turbine performance. J. Eng. Gas Turbines Power **135**(10), 102603/1–102603/9 (2013)